Fuel 235 (2019) 167–177

Contents lists available at ScienceDirect

Fuel

journal homepage: www.elsevier.com/locate/fuel

Full Length Article

NMR relaxometry a new approach to detect geochemical properties of organic matter in tight shales

Seyedalireza Khatibi[a,*], Mehdi Ostadhassan[a,*], Z. Harry Xie[b], Thomas Gentzis[b], Bailey Bubach[a], Zheng Gan[b], Humberto Carvajal-Ortiz[b]

[a] University of North Dakota, Grand Forks, ND 58203, United States
[b] Core Laboratories, 6316 Windfern Road, Houston, TX 77040, United States

ARTICLE INFO

Keywords:
Unconventional reservoirs
Bakken Formation
NMR relaxometry
NMR T_1-T_2 map
Rock-Eval pyrolysis

ABSTRACT

Understanding organic matter properties in terms of maturity and production potential are crucial for the initial assessment of unconventional plays. This is important since the amount of hydrocarbon that can be generated is a function of organic matter type and content in the formation and its thermal maturity. The complexity of shale plays in terms of constituent components has demonstrated that new analytical methods should be acquired to better understand hydrocarbon generation processes. In this study, a few samples from the upper and lower members of the Bakken Formation in the USA were selected from different depths and maturity levels. The samples were analyzed by a high frequency (22 MHz) nuclear magnetic resonance (NMR relaxometry) equipment, followed by Rock-Eval pyrolysis (using the Basic/Bulk-Rock method for all samples and a multi-heating rate method, MHR, for the two least mature samples) and bitumen reflectance evaluations. Results showed NMR can detect different hydrogen populations within the samples and distinguish among phases, such as solid organic matter, hydrocarbons (mobile oil), and water by T_1-T_2 mapping. We were also able to relate different identified areas on NMR T_1-T_2 maps to geochemical parameters of the organic matter obtained from Rock-Eval pyrolysis (such as S1, S2, and HI) and with thermal maturity (vitrinite reflectance-equivalent).

1. Introduction

The amount of hydrocarbons generated from organic matter in a source rock depends on different parameters, such as kerogen type, maturity levels, the total amount of organic carbon [38]. The common methods for evaluating above parameters are programmed pyrolysis and organic petrography by microscopic methods. Open-system programmed pyrolysis or Rock-Eval pyrolysis (RE) is a widely accepted geochemical technique that measures four components related to the main major classes of organic constituents (S1–S4) [33,6,14].

The increase in exploration and production of unconventional reservoirs and their complexity has led to the employment of new methods for resource-play assessment, such as nuclear magnetic resonance (NMR). Solid state ^{13}C nuclear magnetic resonance (NMR) spectroscopic methods have been used extensively to study the decomposition of organic matter in a wide range of media, such as sewage [3], co-composting and bio-wastes [2], kerogen degradation [39], and recent sediments and soils [12]. NMR techniques contribute to the understanding of hydrocarbon resource-plays by studying the behavior and occurrence of petroleum accumulations. NMR techniques have the potential to characterize kerogen [60,28,36,59,11], bitumen [18,52], petroleum [5,32], and asphaltenes [34,5,17]. Tinni et al. [57] used NMR to characterize the mobility of fluids in both conventional and unconventional reservoirs. NMR has the advantage to determinate pore size distribution and liquid typing and saturation analysis [29,15,46,4,40]. It can provide information to confidently infer pore sizes to the nano-meter scale, as well as distinguishing different hydrogen (proton) populations associated to the presence of water, oil, gas, and kerogen [53,56,7]. Fleury and Romero-Sarmiento [20] quantified the connectivity of the pore network system and provided a measure of tortuosity.

Recently, Birdwell and Washburn [8] demonstrated, using multiple techniques to study hydrocarbons in shales, that their NMR data did not show any quantitative correlation with Rock-Eval pyrolysis due to the low sensitivity of the NMR spectrometer (2 MHz) used and the poor resolution in the T_1-T_2 maps. Romero-Sarmiento et al. [42] demonstrated that NMR T_1-T_2 maps, and particularly the T_1/T_2 ratio, can be used to distinguish bitumen, oil, and organic matter as shown in the

* Corresponding authors.
E-mail addresses: Seyedalireza.Khatibi@und.edu (S. Khatibi), mehdi.ostadhassan@engr.und.edu (M. Ostadhassan).

https://doi.org/10.1016/j.fuel.2018.07.100
Received 24 May 2018; Received in revised form 20 July 2018; Accepted 22 July 2018

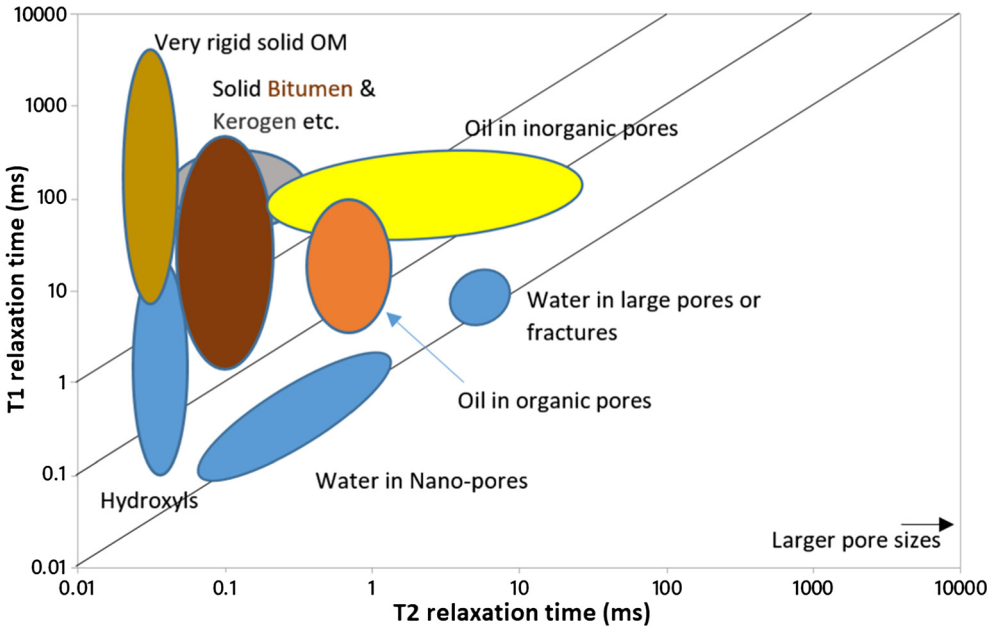

Fig. 1. General map of T_1-T_2 map (modified after Fleury et al. (2016), Romero-Sarmiento et al. [42], Washburn and Birdwell [59], Mehana and El-monier [37].

Jurassic-age Vaca Muerta Formation in Argentina. The above study correlated TOC obtained from Rock-Eval pyrolysis (using the IFPEN Shale Play® method) to 'solid echo' signal intensities calculated by the low field hydrogen NMR relaxometry technique. One of the main challenges still not solved is defining the margins of different components of organic rich shales in T_1-T_2 map that might overlap.

In the present study, the high frequency (22 MHz) NMR relaxometry technique was used as a new approach to identify hydrocarbon components and organic matter in tight shale samples and to establish a relationship between the NMR T_1-T_2 map and Rock-Eval pyrolysis parameters as well as thermal maturity. The proposed method provides a non-destructive complement to evaluate organic matter properties in relatively larger quantities, when compared to conventional methods that use only milligrams of sample. The method also combines geochemical and petrophysical data to better define the location of different components in the T_1-T_2 map.

2. Geological setting of the studied area

The Bakken Formation is an organic-rich shale, mudstone and sandstone that was deposited during the Late Devonian and Early Mississippian periods. It is located in the Williston Basin, USA and extends into Canada [51]. Studies have shown that marine kerogen Type II is the most abundant organic matter in the Bakken [55,27,35,30,1]. Samples from the Bakken Formation were retrieved from six different wells (Wells 1–6) varying in depth and thermal maturity.

3. Analytical methods

3.1. Reflectance measurements

For petrographic analysis, six whole-rock samples were crushed to 20 mesh (850 μm) particles, mixed with Epo Thin epoxy resin and hardener (ratio of 2:1) and left to harden under vacuum conditions for 24 h [23]. The samples were polished using Buehler EcoMet/AutoMet 250 automated polishing equipment. A Carl Zeiss Axio Imager A2m microscope, equipped with a white light source and a UV light was used

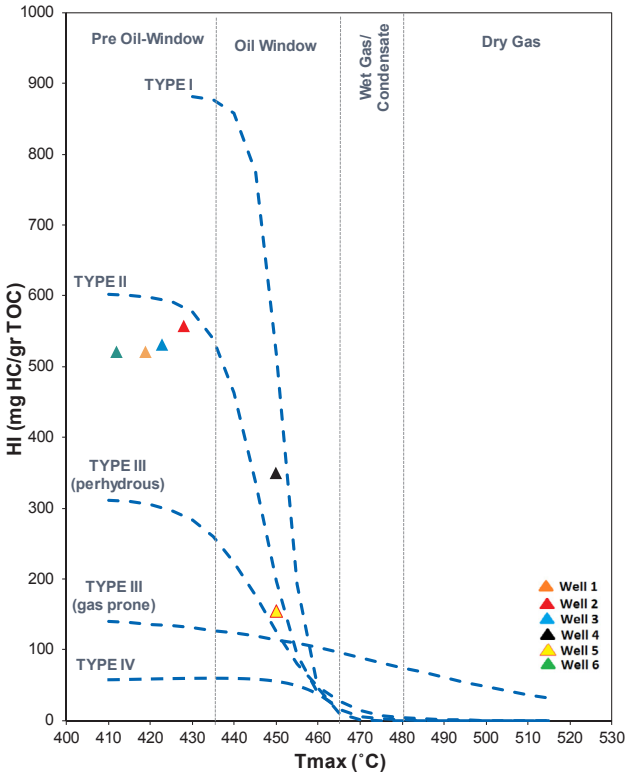

Fig. 2. HI vs. Tmax is showing the type of kerogen in the six samples of this study.

to analyze the random reflectance and qualitative fluorescence, for reflectance measurements and visual kerogen analysis. Due to the absence of primary vitrinite, the equivalent vitrinite maturity %*VRo – eq* was calculated from the reflectance of solid bitumen (%*BRo*) present in the samples using the Jacob [26] formula:

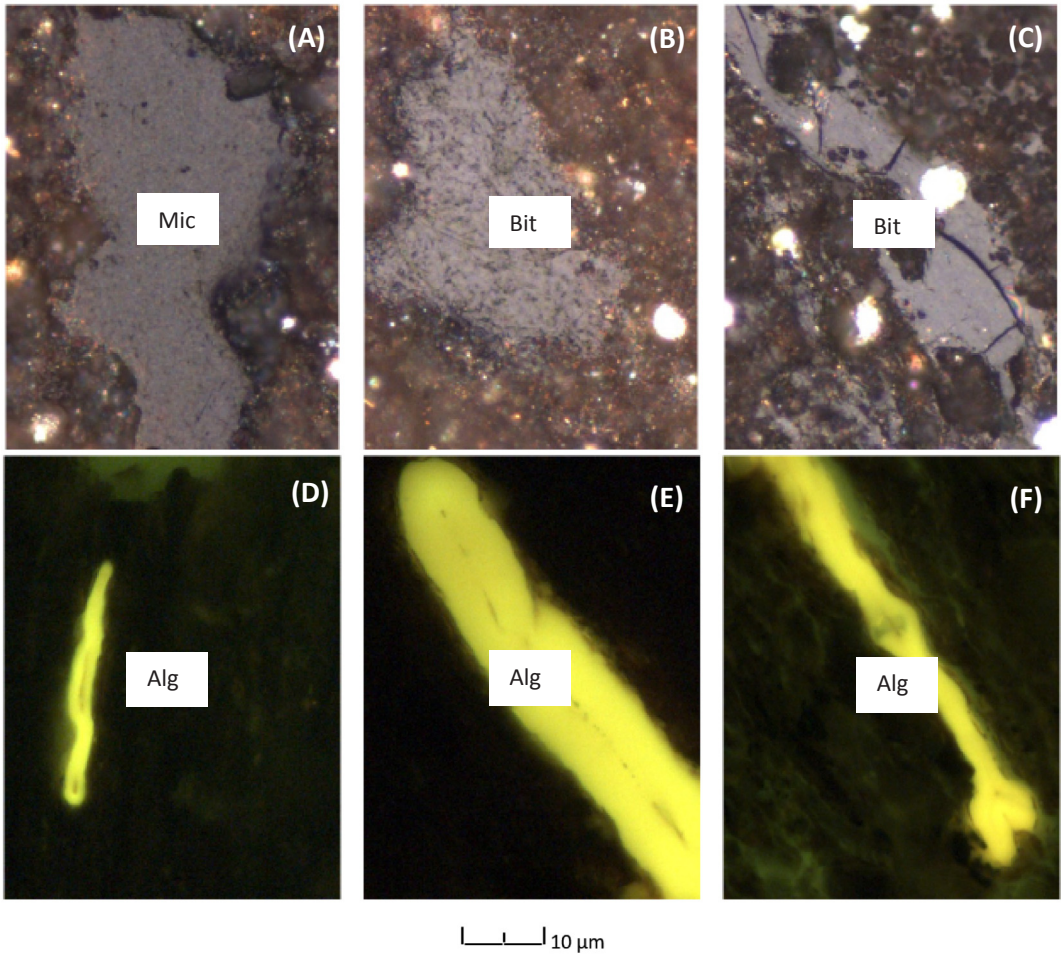

Fig. 3. (A) Micrinite (Mic) showing granular texture (Ro = 0.54%), 5438 ft; (B) Bitumen (Bit) with Ro of 0.50%, 8325 ft; (C) Bitumen (Bit) with Ro of 0.80%, 10,437 ft; (D) Alginite (Alg) having greenish-yellow fluorescence, 5438 ft; (E) A large oil-prone Tasmanites alginite (Alg) exhibiting golden-yellow fluorescence color, 8325 ft; (F) Alginite (Alg) showing golden-yellow fluorescence, 8325 ft. Scale bar is 10 µm. Excitation is at 465 nm; combined dichroic and barrier filter have a cut at 515 nm. Total magnification of photos A-C is 500X and the total magnification of photos D-F is 250X. (For interpretation of the references to color in this figure legend, the reader is referred to the web version of this article.)

Table 1
Rock-Eval data for the six samples using the Basic/Bulk-Rock method.

Basic/Bulk-Rock	Well	Depth (ft)	TOC (wt%)	S1 (mg HC/g)	S2 (mg HC/g)	S3 (mg CO2/g)	S3 (mg CO/g)	T_{max} (°C)	HI (S2 × 100/TOC)	BRO% (%)	VRo-eq (%)
	1	5438	24.71	7.97	128.71	2.08	1.66	419	520.88	0.16	0.38
	2	8325	16.27	8.27	90.69	0.35	4.5	428	557.41	0.22	0.54
	3	9886	15.76	9.27	83.7	0.08	0.25	423	531.09	0.30	0.59
	4	10,437	13.39	7.64	46.79	0.04	0.2	448	349.44	0.74	0.86
	5	10725.5	9.04	6.13	13.94	0.11	0.2	450	154.2	0.87	0.94
	6	3785	14.64	3.4	76	0.41	0.71	412	519.5	0.10	0.25

$$\%VRo\ (equivalent) = \%BRo * 0.618 + 0.4 \quad (1)$$

3.2. Rock-Eval pyrolysis

Crushed samples varying in weight from 15 to 60 mg were subjected to pyrolysis using a Rock-Eval 6 Turbo analyzer (Vinci Technologies, France) via the Basic/Bulk-Rock method (IFP methods). Each sample was placed in the pyrolysis oven and heated isothermally for 3 min at 300 °C before the temperature was increased to 650 °C at a rate of 25 °C/min. In addition, the least mature and shallowest samples from Well 1 and Well 6 were analyzed using a modified IFP Shale Play® method, referred to therein as multi-heating rate (MHR) method. The initial heating temperature was 100 °C and was increased to 200 °C where it was kept isothermal for 3 min in order to complete the thermal extraction of the lightest hydrocarbon fraction (Sh0; C1-C15

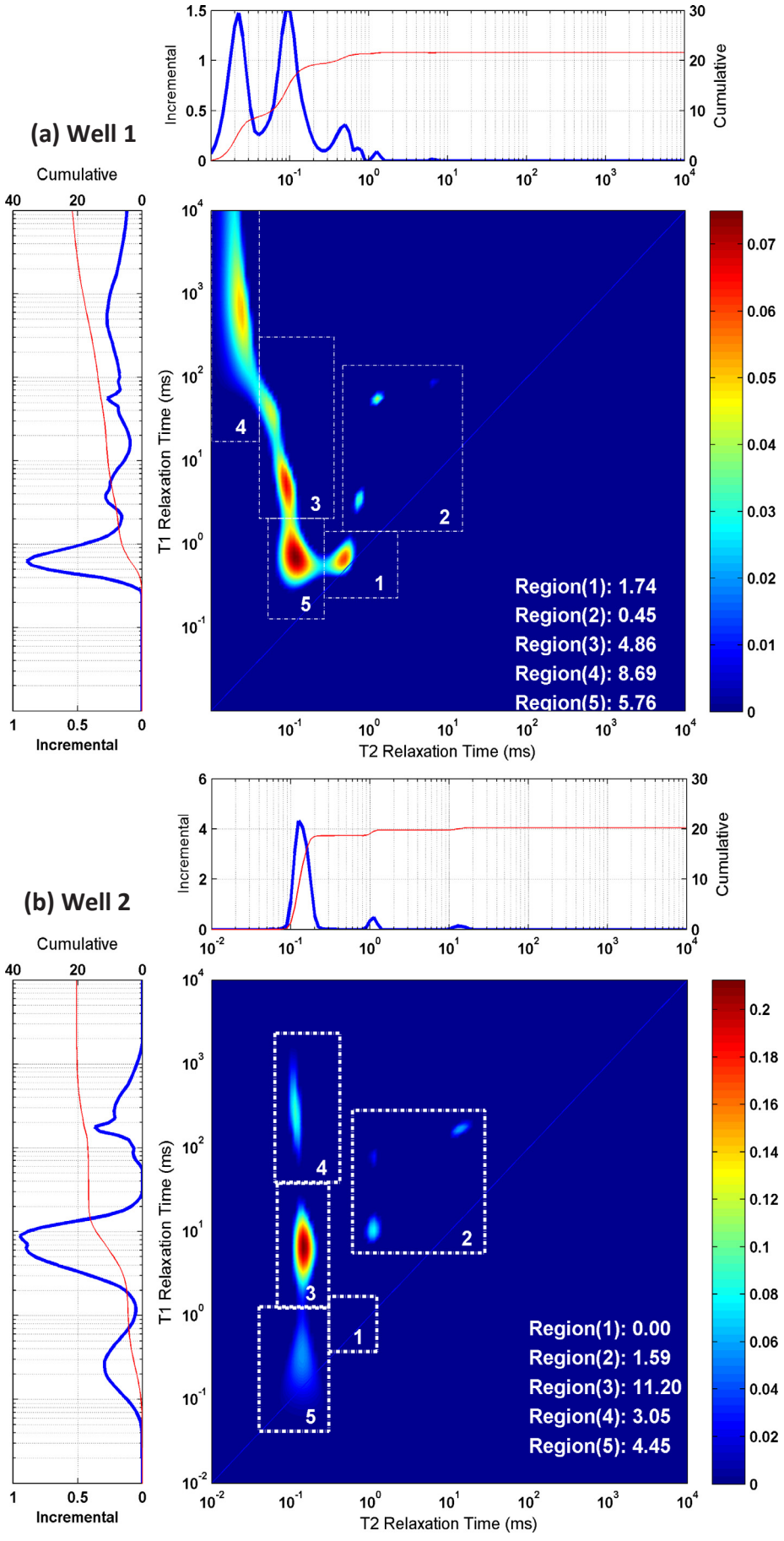

(caption on next page)

Fig. 4. (a–f): T1-T2 maps for Well 1 to Well 6. Regions (1)–(5) and their corresponding amplitudes (NMR Hydrogen fraction (mg/g)) are shown on each map. A cut-off of T2 = 0.05 ms derived from Well 1 and Well 5, was applied to Well 4 to separate Regions (3) and (4). 1-D distributions of relaxation times for each map are also shown at the top and left side (blue is incremental and red is cumulative), which represent the intensity projection of the map on each axis. Signal amplitudes are expressed in a unit of milligram hydrogen per gram rock sample (mg H/g rock). It should be mentioned that the blue curve is incremental, and the red curve is cumulative. (For interpretation of the references to color in this figure legend, the reader is referred to the web version of this article.)

hydrocarbons) [45,44,13]. From 200 °C, the oven temperature was increased to 350 °C at 25 °C/min, staying isothermal for 3 min for the thermal extraction of the medium-heavy hydrocarbon fraction (Sh1; C15-C40 hydrocarbons; [50]). The last temperature step consisted of ramping the temperature to 650 °C at 25 °C/min for the thermal cracking of the NSO and/or kerogen fraction (Sh2; [45,50]). For more details, the reader is referred to Romero-Sarmiento et al. [45,44,43] and Carvajal-Ortiz and Gentzis [13].

3.3. NMR relaxometry

When dealing with unconventional formations, such as shale oil or shale gas with the characteristics of low porosities, very small pores, co-existence of water, oil and other organic matter and ultra low permeability, the traditional low frequency NMR is insensitive and unable to detect fast decay signals from solid organic matter or distinguish between water and oil.

Since it was first launched commercially in 2013, high frequency (HF, at 22 MHz) NMR techniques have quickly gained attention and acceptance in the unconventional rock core analysis as a means to obtain quality petrophysical properties. HF NMR has the advantages of 30–50-fold more sensitivity than low frequency (usually 2 MHz or lower) NMR and much shorter inter-echo spacing time. These make the HF NMR an ideal tool to characterize unconventional mudstones because of its capability to detect hydrogen signals not only from water and oil but also from solid organic matter.

The two-dimensional NMR mapping techniques [54], i.e., T_1-T_2 correlation measurements, have gradually gained attention in the petroleum for advantages in plotting both relaxations time T_1 and T_2 simultaneously. Previous studies have shown the general location of different components in the T_1-T_2 map [21,19,59,20]. The summary of previous studies on the general location of different components in T_1-T_2 map is shown in Fig. 1. The boundary of regions in the 2D map might overlap and cannot be defined clearly. T_1 in organic solids is long because the frequency of fluctuations in solids are inefficient at transferring energy to the environment and cause overlapping of signals, while T_2 relaxation times will be shorter due to the strong intramolecular dipolar coupling that quickly dephases the spins.

Generally, T_2 is the measure of molecular mobility. The longer is the T_2, the more mobile the molecules are. Therefore, signal regions on the right side of the map are from mobile components or from liquids in large pores, and on the left side are from more bound and more viscous liquids, from liquids in small pores, or from solid components. This leads to a direct result that T_2 relaxation is inversely proportional to viscosity [16]. A decrease in viscosity is equivalent to an increase in T_2 relaxation time if the liquids are present in similar size pores. Water, oil and solid organic matter can be identified with the ratios of T_1 and T_2 according to the Bloembergen-Purcell-Pound (BPP) theory and according to the molecule sizes relative to pore sizes. BPP theory is a theoretical model of NMR relaxation mechanism proposed by [9]. The theory explained the NMR relaxation constants (i.e. relaxation times, T1 and T2) of a pure substance in correspondence with its state, taking into account the effect of tumbling motion of molecules on the local magnetic field disturbance. The theory is in good agreement with numerous experiments on pure substances and complex compounds such as porous media with some exceptions.

In the present study, the NMR measurements were made at Core Laboratories with a customized22MHz spectrometer from MR Cores, equipped with a 30 mm diameter probe, which is configured to have a very short ring down delay time (or “dead time”) of less than 15 μs to allow for early time NMR data acquisition. This will enable us to capture signals from solid components with a very short T2 in the sample. The NMR probe size allowed for measurements on samples of any shape or form that can be loaded into sample vials of 30 mm diameter. All samples in this study were shale fragments ranging from 12 g to 20 g in weight. The T_2 data were acquired using the CPMG sequence with an echo time spacing of TE = 0.07 ms. The T_1 data were acquired using an inversion-recovery sequence. The T_1-T_2 correlation data were acquired using a pulse sequence of combining T_1 and T_2 data acquisitions, where 61 T1 wait steps were used and 5000 echoes were recorded at each T1 wait step, then processed using an Optimized Truncated Singular Value Decomposition (OTSVD) inversion method [24,25,62] to obtain the 2D T_1-T_2 map. A standard sample of a known amount of water mixed with D_2O sealed in a glass vial was used to calibrate the NMR instrument for quantitative data acquisition.

4. Results and discussion

4.1. Rock-Eval pyrolysis and organic petrography

Pyrolysis results (Fig. 2) and organic petrography study of the samples (Fig. 3) show that organic matter type II is the main constituent of the organic facies. It should be noted, scale bar is 10 μm in Fig. 3; excitation is at 465 nm; combined dichroic and barrier filter have a cut at 515 nm. Total magnification of photos A-C is 500X and the total magnification of photos D-F is 250X. Vitrinite reflectance-equivalent values (converted from bitumen Ro using the Jacob [26] Formula) show that the organic matter in the six wells ranges from immature to approximately the middle part of the oil window (Table 1).

4.2. NMR 2-D mapping

T_1-T_2 maps for the six samples (Well 1 to Well 6) were generated. The samples were in their native form. The maps are shown in Fig. 4(a–f). In order to obtain quantitative information in each component on a T1-T2 map, T1 and T2 values as borders of the boxes are needed to be selected which are culled cut-offs. In normal cases, these borders (cut-offs) are clearly defined on a T1-T2 map, e.g. regions (1) and (2). But exceptions are quite often, e.g. regions (3) and (4) for the well 4, where knowledge of physical properties, such as T1 and T2, of heavy hydrocarbons will be applied. It is also one of our goals to use Rock-Eval data to help us to define cut-offs for each region on a T1-T2 map.

In order to compare the NMR measurements with Rock-Eval pyrolysis and thermal maturity analysis, five regions on the map were identified, as shown in Fig. 4. In reference to Section 3.3 and also Fig. 1 as a general guide, Region (1) in Fig. 4 shows a T_1/T_2 ratio close to 1, so it represents water in nano-pores. Region (2) is in the oil position

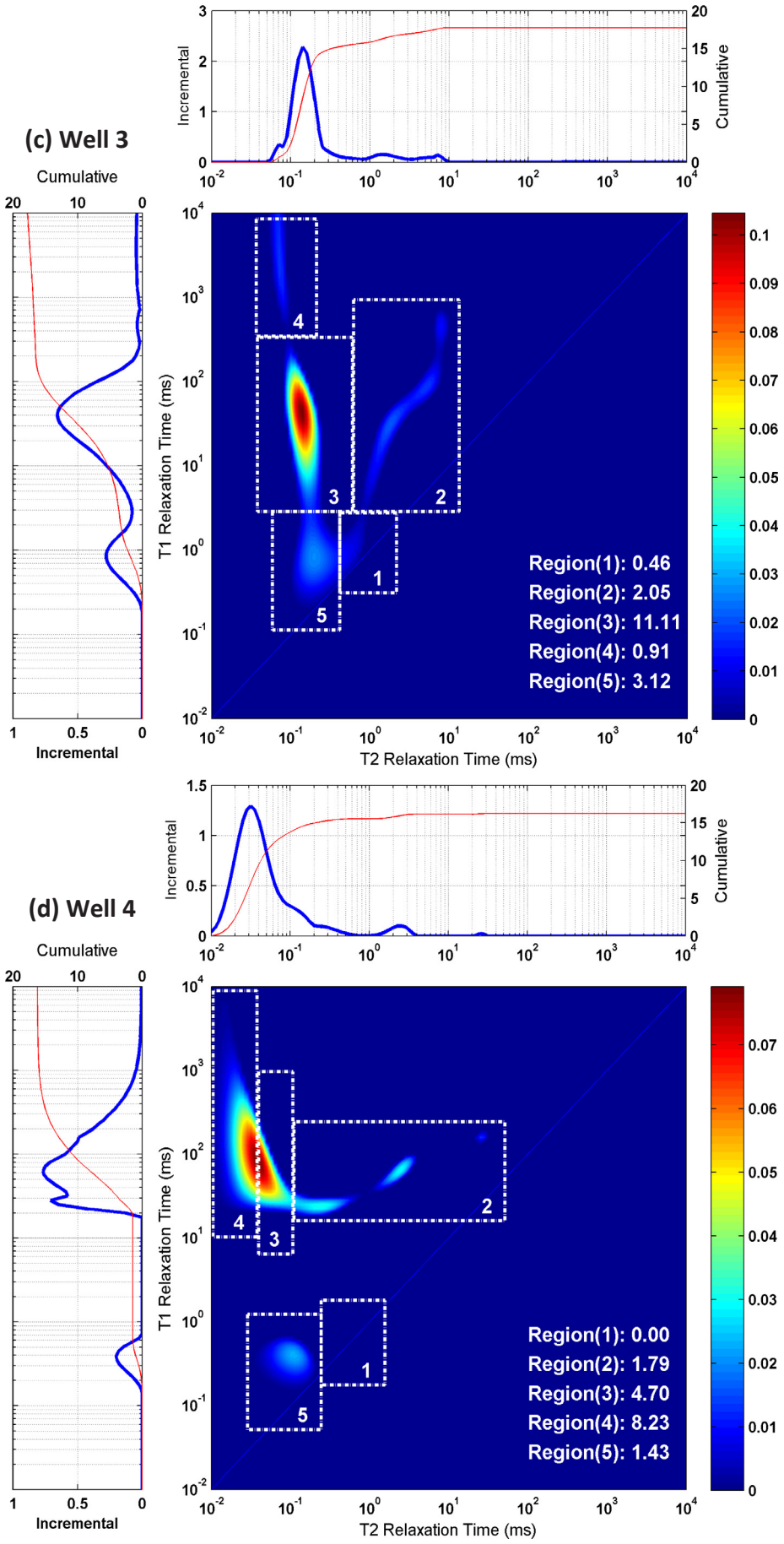

Fig. 4. (*continued*)

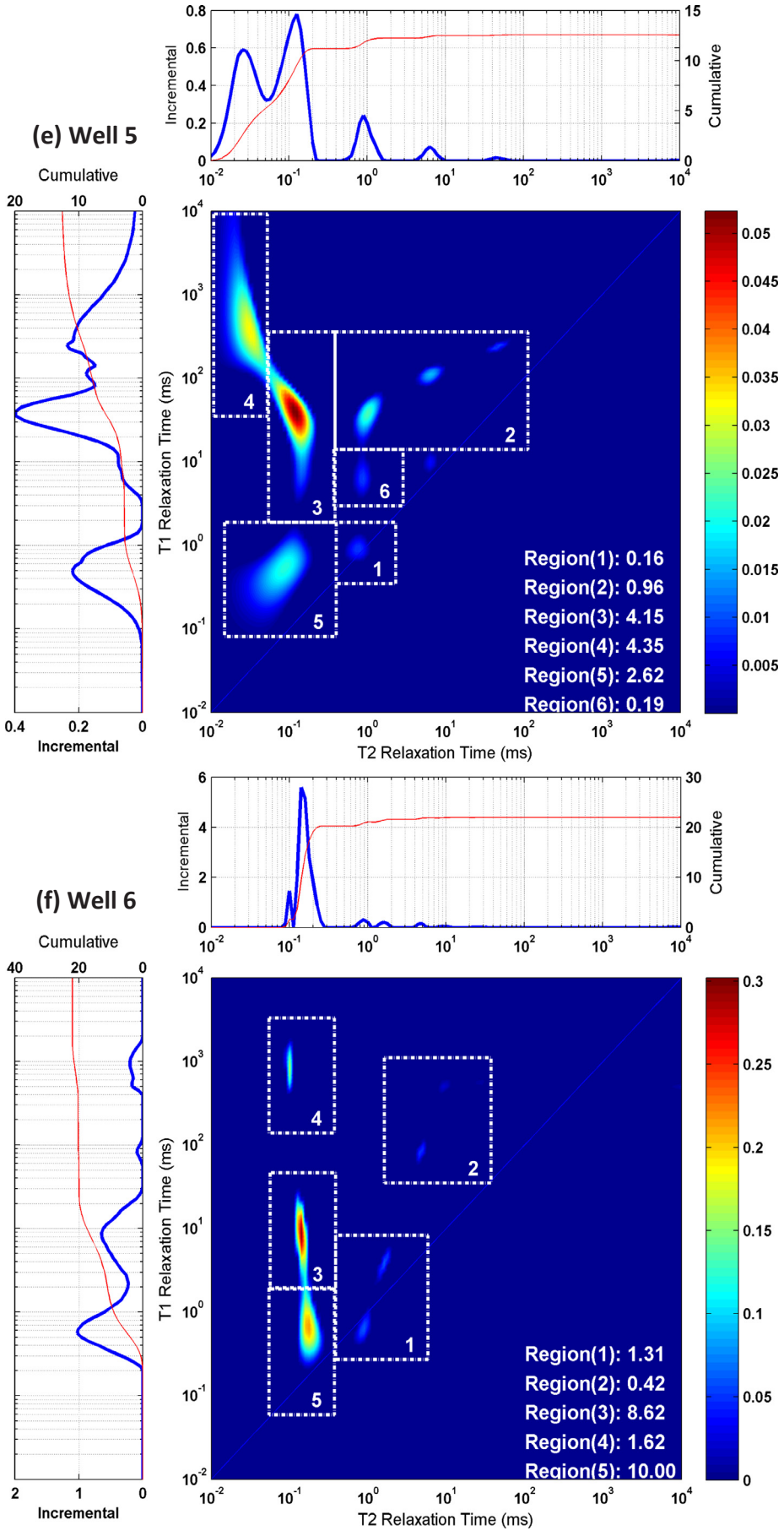

Fig. 4. (*continued*)

Table 2
Amplitude of the NMR signal of regions 1–5 and T_1/T_2 ratios.

Well No.	NMR Signal Amplitude (mg H/g)						Region (3) on the Maps		
	Region (1)	Region (2)	Region (3)	Region (4)	Region (5)	Region (6)	T_1 (ms)	T_2 (ms)	T_1/T_2
1	1.74	0.45	4.86	8.69	5.76	0	5.5	0.09	61.11
2	0.00	1.59	11.20	3.05	4.45	0	9.4	0.11	85.45
3	0.46	2.05	11.11	0.91	3.12	0	21.4	0.16	133.75
4	0.00	1.79	4.70	8.23	1.43	0	48.6	0.15	324.00
5	0.21	1.15	4.15	4.35	2.62	0.19	44.7	0.11	406.36
6	1.31	0.42	8.62	1.62	10.00	0	8.5	0.14	60.71

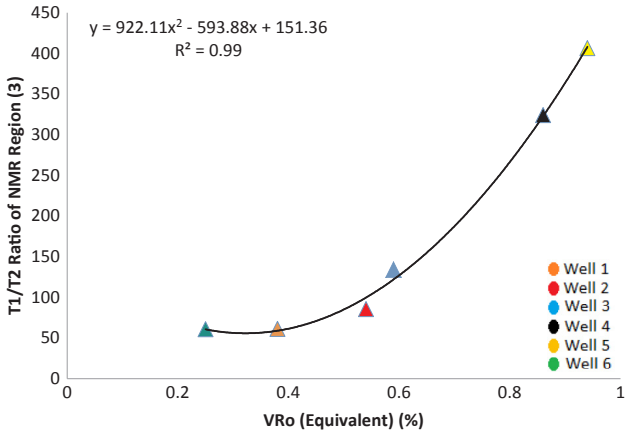

Fig. 5. T_1/T_2 ratio of Region 3 from the NMR T_1-T_2 map vs. maturity (VRo equivalent). The trend shows the T_1/T_2 ratio increases with thermal maturity. The power function relationship has a correlation coefficient (R^2) value of 0.99 including all samples.

indicating moveable oils. Region (3) has a higher T_1/T_2 ratio, T_2 is very short, and represents heavy oil or solid organic matter. Region (4) has the highest T_1/T_2 ratio and shortest T_2; it comes from very rigid solids that contain hydrogen. Region (5) has a small T_1/T_2 ratio with a very short T_2, it most likely comes from water in nano-pores, hydroxyl, or organic matter. This may be identified in combination with pyrolysis data. Region (6) in Fig. 4(e) is from oil in organic pores and can be part of Region (2). The amplitudes and values of T_1 and T_2 from each region are summarized in Table 2.

It should be noted that Region (4) on the T_1-T_2 maps for Wells 1, 4, and 5 has very short T_2s. This is thought to be caused by the existence of strong paramagnetic impurities in the samples. The Bakken Formation is known to contain pyrite and other iron-bearing minerals, such as ilmenite (Fe_3O_4) and chlorite, as well as halite which reduce the relaxation time T_2 [47].

4.3. Correlations between NMR and pyrolysis

We believe NMR can reveal the maturity stage of organic matter indirectly. As organic matter matures, it loses aliphatic chains (the portion with high hydrogen content) and becomes more aromatic [31]. Aromatic rings form clusters, which makes the solid organic matter more rigid. Thus, the T_1 relaxation times of organic matter are expected to be longer when it becomes more thermally mature [10,59]. On the other hand, the solid organic matter shows T_2 at almost constant value. Thus, the T_1/T_2 ratio in Region (3) is expected to increase when maturity (as reflected by VRo-equivalent) increases, as shown in Fig. 5. The correlation between T_1/T_2 ratio vs. VRo (equivalent) using the second order polynomial fit is almost perfect for all samples including the two immature ones.

Another way to correlate NMR data to VRo (equivalent) is by using the amplitude of Region (3) representing solid organic matter. Fig. 6 displays the above relationship. As seen, as maturity increases, the amplitude of Region (3) – representing hydrogen content - decreases, which in accordance to the general trend of maturation of organic matter. However, the two immature samples (Well 1 and Well 6) are shown as outliers, a behavior that will be discussed in the following paragraphs. It should be emphasized that the hollow triangle or square symbols in the following figures represent the wells that have not been used in the regression process.

It was stated earlier that NMR can present data from different sources of hydrogen population in the samples. Therefore, the hydrogen population that represents the organic matter zones in the T_1-T_2 map could be correlated to the Hydrogen Index (HI) from Rock-Eval pyrolysis, as seen in Fig. 7, which is also in accordance with Fig. 6. Since, as

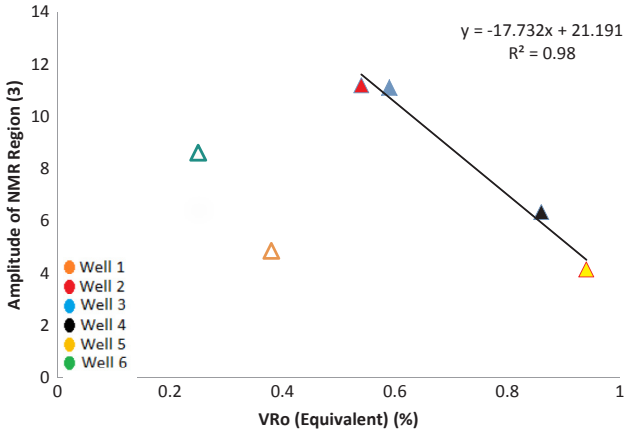

Fig. 6. Hydrogen volume of Region 3 in the NMR T_1-T_2 map vs. VRo (equivalent) from Petrography. The correlation coefficient of samples excluding two immature ones is 0.98.

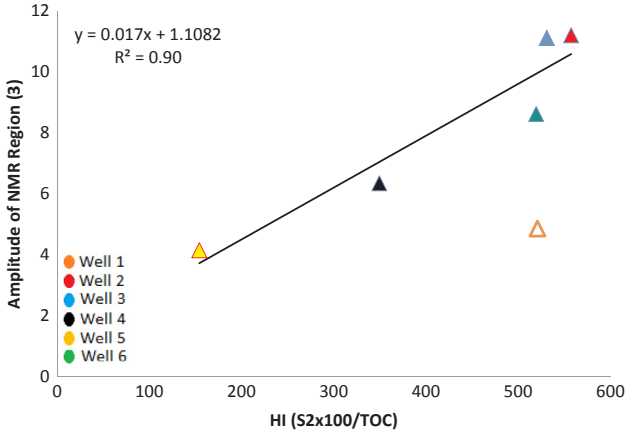

Fig. 7. Hydrogen volume (mg H/g rock) of Region 3 in the NMR T_1-T_2 map vs. HI from Rock-Eval. The linear relationship with correlation coefficient 0.90 excluding Well 1.

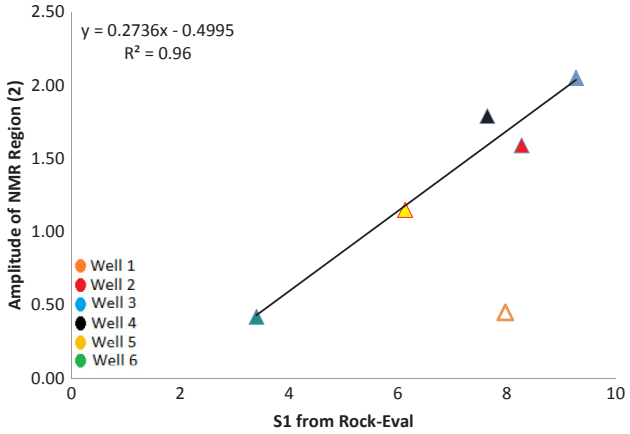

Fig. 8. Hydrogen volume (mg H/g rock) of Region 3 in the NMR T_1-T_2 map vs. S1 from Rock-Eval. The linear relationship with correlation coefficient 0.96 excluding Well 1.

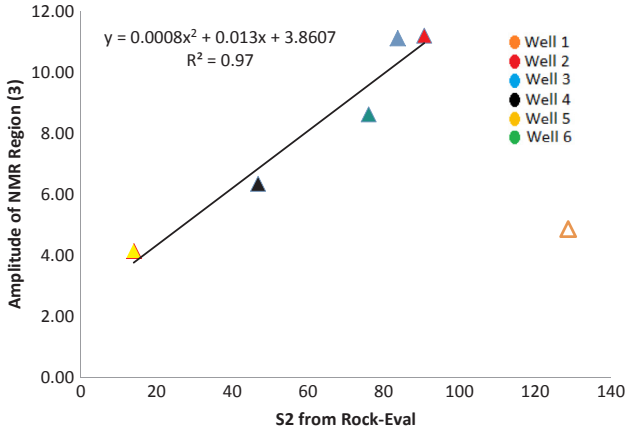

Fig. 9. Hydrogen Volume of Region 3 in the NMR T_1-T_2 map vs. S2 HC volume from Rock-Eval, with correlation coefficient 0.97 excluding Well 1.

maturity increases, hydrogen content of organic matter decreases, thus the amplitude of Region (3) decreases. So, maturity has a reverse and HI has a direct trend with the amplitude of Region (3).

NMR can provide an improved understanding of S1 and S2 peaks in Rock-Eval pyrolysis. Since S1 is defined as the free hydrocarbons present in pores, it can be correlated to the hydrogen fraction (population) measured by NMR from the oil region (Region 2) in T_1-T_2 maps, as seen in Fig. 8. The immature sample in Well 1 is clearly an outlier. On the other hand, S2 in Rock-Eval is the potential of source rock to generate hydrocarbons upon heating. Molecular structures with higher hydrogen content, such as aliphatic ones, contribute the most to the conversion of organic matter to hydrocarbons [61,22]. Accordingly, the hydrogen content in organic matter can be directly correlated to the S2 from Rock-Eval. Fig. 9 shows the relationship between the amplitude of Region (3) vs. S2. The immature sample in Well 1 is still an outlier.

As seen, NMR spectroscopy shows high potential in correlating different regions on the T_1-T_2 map to thermal properties of organic matter, except for two immature samples. In order to reason out this challenge, different causes were considered.

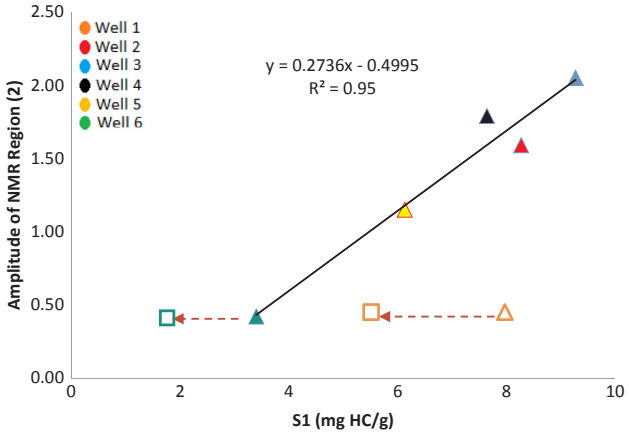

Fig. 10. Hydrogen volume (mg H/g rock) of Region 3 in the NMR T1-T2 map vs. S1 from Rock-Eval. Squares are the corresponding Sh0 from MHR method.

Firstly, we substituted S1 from the Basic/Bulk-Rock method for Sh0 from the MHR method for the immature samples in Well 1 and Well 6. The MHR method captures those light hydrocarbons that otherwise would be volatilized and not measured by the Basic/Bulk-Rock method in immature samples containing the highest amount of thermo-vaporizable light hydrocarbons. Using the MHR pyrolysis method (Table 3) resulted in the data points of the immature samples shifting to the left in the correlation with Region 2 from NMR. Well 1 moved closer to the trend line of the other five samples while this was not the case for Well 6 (Fig. 10). Following the same idea, S2 and HI from the Basic/Bulk-Rock method can also be replaced with corresponding values in the MHR method. However, no major changes occurred in the values (compare Tables 1 and 3.

Another explanation which seems to be the dominant reason for such a behavior of Well 1 and Well 6 would be the overlapping boundaries of regions. Boundaries can be affected by the maturity level of organic matter, mineralogy, and the presence of magnetic minerals.

On the NMR maps of the two immature samples (Well 1 and Well 6), Region (5) has much more hydrogen signals than the other samples. As shown before, T_1/T_2 ratios of immature samples are low, while T_1 relaxation times of hydroxyl signals are very long, so at low maturity levels organic matter signal might overlap with the signal from hydroxyl, i.e., some organic signals shift to Region (5) in the T_1-T_2 map. Some minerals have hydroxyl groups (OH) in their structure, for example, ripidolite with a formula of $(Mg,Fe,Al)_6(Si,Al)_4O_{10}(OH)_8$ or illite having a formula of $K(Al_2)(Si_3AL)O_{10}(OH)_2$. Kerogen has also OH group in its structure [58,41]. This could explain the reason for the outlier behavior of Well 1 and 6 in Fig. 6. Finally, it is seen that both Well 1 and Well 6 did not follow the overall observed trend in the cross-plot of % VRo and the amplitude of region 3 of NMR maps. As explained earlier, this is inferred possibly due to the overlapping of signals between region 3 with the OH signals that should appear in Region 5. However, Well 6 started to follow the trend of other samples in the S1 and S2 peaks vs. Region 3 amplitude which made us to believe mineral content of the samples could possibly play an important role on the results.

To understand the chemical and mineralogical composition of the Bakken shale in high-resolution scale, the newly developed EDS (energy dispersive spectrometry) and backscattered electron (BSE) analysis were carried out on the samples. By a combination of the EDS and BSE

Table 3
Data for the two immature samples processed using the MHR method.

Multi-heating method	Well	TOC (wt%)	Sh0 (mg HC/g)	Sh1 (mg HC/g)	OIL (mg HC/g)	Sh2 (mg HC/g)	S3 (mg CO2/g)	HI (Sh2 × 100/TOC)	OI (S3 × 100/TOC)
	1	25.79	5.51	9.1	14.61	126.17	0.16	489.22	0.62
	6	14.64	1.72	5.74	7.46	75.55	0.19	516	2.97

Table 4
XRD data of Wells 1–5 showing wt% of different minerals.

Mineral (wt%)	Well 1	Well 2	Well 3	Well 4	Well 5	Well 6
Quartz	6.08	44.66	43.28	77.59	26.57	39.1
Alkali Feldspar	32.41	43.23	42.23	14.22	36.18	12.6
Plagioclase	2.27	0.7	0.52	0.38	1.19	4.2
Biotite	10.35	0.31	0.19	0.16	0.7	0
Muscovite	3.91	0.43	0.58	0.2	0.82	15.5
Illite	36.67	5.67	6.37	1.13	12.62	10.3
Chlorite	0.35	0.11	0.09	0	0.16	1.31
Zircon	0.01	0.01	0.01	0	0.01	0
Calcite	0	0.39	0.21	0.58	0.81	1.5
Siderite	0	0	0.03	0.05	0.04	0
Dolomite	1.05	0.85	0.69	1.76	12.62	2.2
Ankerite	0.41	0.34	0.22	0.7	3.34	0
Apatite	0.21	0.08	0.19	0.05	0.08	1.2
Monazite	0.31	0	0	0	0.01	0
Pyrite	5.71	3.05	5.23	3.07	4.62	3.84
Rutile	0.2	0.15	0.17	0.1	0.2	0
Ilmenite	0.05	0	0	0	0	0
Halite	0	0	0	0	0	1.79
Marcasite	0	0	0	0	0	6

results, a 2-D high-resolution mineralogical map of every single layer of the sample [49] could be created. Chemical mapping provides the ability of better differentiation between various types of any individual mineral with a high degree of accuracy such as Na-Ca plagioclases and especially clay minerals. MAPS Mineralogy (Modular Automated Processing System; [48,49]) indicated that quartz, alkali feldspars, plagioclase, illite, pyrite, biotite, and muscovite are the most abundant minerals of the Bakken shales. As seen in Table 4, Well 1 has high Illite content. Moreover, ilmenite is also a magnetic mineral, which is only present in the Well 1 sample. Thus, it can be concluded that Well 1, due to having the lowest maturity and high content of magnetic minerals and minerals with OH group in their structure, shows a different trend.

The proposed method is a fast and non-destructive way to understand kerogen thermal properties in terms of programmed pyrolysis. Furthermore, the minimal and rapid sample preparation for high frequency NMR enables us to evaluate such properties in a quick method even at the well site. In future studies, different samples from different formations and higher maturity levels would be evaluated to assess the potential of such a method.

5. Conclusions

The following conclusions can be drawn from this limited-in-scope study:

- The T_1/T_2 ratio in Region (3) on NMR T_1-T_2 maps shows a positive trend with increasing thermal maturity, as expressed by vitrinite reflectance (equivalent) which is also robust in low mature samples.
- The amplitude of the Region (3) on NMR T_1-T_2 maps (related to organic matter) shows a strong correlation with VRo (equivalent), which is not applicable in low mature samples.
- Positive correlations between NMR and Rock-Eval pyrolysis S1 values for samples in the oil window were obtained. This means that NMR can be used to identify and correlate hydrocarbons (mobile oil) in Region (2) of the T_1-T_2 map against the S1 parameter.
- NMR 'solids' (viscous solids containing NSO compounds) in Region (3) of the T_1-T_2 map can be correlated to the S2 parameter from programmed pyrolysis.
- Region (3) volume shows a positive correlation with Hydrogen Index from Rock-Eval pyrolysis.
- The NMR method used in this study is promising and complementary to the traditional analytical methods, such as Rock-Eval pyrolysis and vitrinite reflectance. It shows a great potential and the ability to differentiate between hydrocarbons (mobile oil) versus moveable and non-moveable (solids) components in unconventional shale/mudrock samples. However, low mature samples and those with magnetic minerals might show different trends.
- The Complexity of unconventional shale plays has led to the employment of new analytical techniques. HF NMR can reveal porosity, permeability, and other petrophysical properties of the sample, by adding geochemical parameters to this set of important characteristics using the proposed method, unconventional reservoirs will be better characterized.

References

[1] Abarghani A, Ostadhassan M, Gentzis T, Carvajal-Ortiz H, Bubach B. Organofacies study of the Bakken source rock in North Dakota, USA, based on organic petrology and geochemistry. Int J Coal Geol 2018;188:79–93.
[2] Albrecht R, Joffre R, Le Petit J, Terrom G, Perissol C. Calibration of chemical and biological changes in cocomposting of biowastes using near-infrared spectroscopy. Environ Sci Technol 2009;43:804–11.
[3] Albrecht R, Ziarelli F, Alarcon-Gutierrez E, Le Petit J, Terrom G, Perissol C. 13C solid-state NMR assessment of decomposition pattern during co-composting of sewage sludge and green wastes. Eur J Soil Sci 2008;59:445–52.
[4] Al Hinai A, Rezaee R, Esteban L, Labani M. Comparisons of pore size distribution: a case from the Western Australian gas shale formations. J Unconventional Oil Gas Resour 2014;8:1–13.
[5] Andrews AB, Edwards JC, Pomerantz AE, Mullins OC, Nordlund D, Norinaga K. Comparison of coal-derived and petroleum asphaltenes by 13C nuclear magnetic resonance, DEPT, and XRS. Energy Fuels 2011;25:3068–76.
[6] Behar F, Beaumont Y, De B, Penteado HI. Rock-Eval 6 technology: performances and develeopments. Oil and gas science and technology. Rev Inst Français Pétrole Energ Nouv 2001;56:111–34.
[7] Behroozmand AA, Keating K, Auken E. A review of the principles and applications of the NMR technique for near-surface characterization. Surv Geophys 2015;36:27–85.
[8] Birdwell JE, Washburn KE. Multivariate analysis relating oil shale geochemical properties to NMR relaxometry. Energy Fuels 2015;29:2234–43.
[9] Bloembergen N, Purcell EM, Pound RV. Relaxation effects in nuclear magnetic resonance absorption. Phys Rev 1948;73(7):679–712.
[10] Bryan J, Kantzas A, Moon D. In situ viscosity of oil sands using low field NMR. Canadian International Petroleum Conference. Petroleum Society of Canada; 2003.
[11] Cao X, Birdwell JE, Chappell MA, Li Y, Pignatello JJ, Mao J. Characterization of oil shale, isolated kerogen, and postpyrolysis residues using advanced 13C solid-state nuclear magnetic resonance spectroscopy. AAPG Bull 2013;97:421–36.
[12] Carrie J, Sanei H, Stern G. Standardisation of Rock-Eval pyrolysis for the analysis of recent sediments and soils. Org Geochem 2012;46:38–53.
[13] Carvajal-Ortiz H, Gentzis T. Geochemical screening of source rocks and reservoirs: the importance of using the proper analytical program. Int J Coal Geol 2018;190:56–69.
[14] Carvajal-Ortiz H, Gentzis T. Critical considerations when assessing hydrocarbon plays using Rock-Eval pyrolysis and organic petrology data: data quality revisited. Int J Coal Geol 2015;152:113–22.
[15] Coates GR, Xiao L, Prammer MG. NMR logging: principles and applications. Gulf Professional Publishing; 1999.
[16] Dunn K-J, Bergman DJ, Latorraca GA. Nuclear magnetic resonance: petrophysical and logging applications. Seismic Exploration, 32. Amsterdam, New York: Pergamon; 2002. p. 93.
[17] Dutta Majumdar R, Gerken M, Mikula R, Hazendonk P. Validation of the Yen-Mullins model of Athabasca oil-sands asphaltenes using solution-state 1H NMR relaxation and 2D HSQC spectroscopy. Energy Fuels 2013;27:6528–37.
[18] Feng Y, Le Doan TV, Pomerantz AE. The chemical composition of bitumen in pyrolyzed Green River oil shale: characterization by 13C NMR spectroscopy. Energy Fuels 2013;27:7314–23.
[19] Fleury M. Characterization of shales with low field NMR. In The International Symposium of Core Analysts, Avignon, France, 8e11 September, SCA2014-014; 2014.
[20] Fleury M, Romero-Sarmiento M. Characterization of shales using T 1–T 2 NMR maps. J Petrol Sci Eng 2016;137:55–62.
[21] Fleury M, Kohler E, Norrant F, Gautier S, M'Hamdi J, Barré L. Characterization and quantification of water in smectites with low-field NMR. J Phys Chem C 2013;117:4551–60.
[22] Gao Y, Zou Y-R, Liang T, Peng PA. Jump in the structure of Type I kerogen revealed from pyrolysis and 13C DP MAS NMR. Org Geochem 2017;112:105–18.
[23] Hackley PC, Araujo CV, Borrego AG, Bouzinos A, Cardott BJ, Cook AC, et al. Standardization of reflectance measurements in dispersed organic matter: results of an exercise to improve interlaboratory agreement. Mar Pet Geol 2015;59:22–34.
[24] Hansen PH. The truncated SVD as a method for regularization. BIT 1987;27:534–53.
[25] Hanson RJ. A numerical method for solving Fredholm integral equations of the first kind using singular values. SIAM J Numer Anal 1971;8(3):616–22.
[26] Jacob H. Classification, structure, genesis and practical importance of natural solid oil bitumen ("migrabitumen"). Int J Coal Geol 1989;11:65–79.
[27] Jin H, Sonnenberg SA. Characterization for source rock potential of the Bakken Shales in the Williston Basin, North Dakota and Montana. Unconventional

Resources Technology Conference (URTEC); 2013.
[28] Kelemen S, Afeworki M, Gorbaty M, Sansone M, Kwiatek P, Walters C, et al. Direct characterization of kerogen by X-ray and solid-state 13C nuclear magnetic resonance methods. Energy Fuels 2007;21:1548–61.
[29] Kenyon W. Petrophysical principles of applications of NMR logging. Log Anal 1997;38.
[30] Khatibi Seyedalireza, Ostadhassan Mehdi, Tuschel David, Gentzis Thomas, Bubach Bailey, Carvajal-Ortiz Humberto. Raman spectroscopy to study thermal maturity and elastic modulus of kerogen. Int J Coal Geol 2018;185:103–18.
[31] Khatibi Seyedalireza, Ostadhassan Mehdi, Tuschel David, Gentzis Thomas, Carvajal-Ortiz Humberto. Evaluating molecular evolution of kerogen by raman spectroscopy: correlation with optical microscopy and Rock-Eval pyrolysis. Energies 2018;11(6):1–19.
[32] Korb J-P, Louis-Joseph A, Benamsili LS. Probing structure and dynamics of bulk and confined crude oils by multiscale NMR spectroscopy, diffusometry, and relaxometry. J Phys Chem B 2013;117:7002–14.
[33] Lafargue E, Marquis F, Pillot D. Rock-Eval 6 applications in hydrocarbon exploration, production and soil contamination studies. Rev Inst Français Pétrole 1998;63:421–37.
[34] Lisitza NV, Freed DE, Sen PN, Song Y-Q. Study of asphaltene nanoaggregation by nuclear magnetic resonance (NMR). Energy Fuels 2009;23:1189–93.
[35] Liu K, Ostadhassan M, Gentzis T, Carvajal-Ortiz H, Bubach B. Characterization of geochemical properties and microstructures of the Bakken Shale in North Dakota. Int J Coal Geol 2017.
[36] Mao J, Fang X, Lan Y, Schimmelmann A, Mastalerz M, Xu L, et al. Chemical and nanometer-scale structure of kerogen and its change during thermal maturation investigated by advanced solid-state 13 C NMR spectroscopy. Geochim Cosmochim Acta 2010;74:2110–27.
[37] Mehana Mohamed, El-monier Ilham. Shale characteristics impact on Nuclear Magnetic Resonance (NMR) fluid typing methods and correlations. Petroleum 2016;2(2):138–47.
[38] McCarthy K, Rojas K, Niemann M, Palmowski D, Peters K, Stankiewicz A. Basic petroleum geochemistry for source rock evaluation. Oilfield Rev 2011;23:32–43.
[39] Petsch ST, Smernik RJ, Eglinton TI, Oades JM. A solid state 13C-NMR study of kerogen degradation during black shale weathering. Geochim Cosmochim Acta 2001;65:1867–82.
[40] Piedrahita J, Aguilera R. Estimating oil saturation index OSI from NMR logging and comparison with Rock-Eval pyrolysis measurements in a shale oil reservoir. SPE Unconventional Resources Conference. Society of Petroleum Engineers; 2017.
[41] Raja MA, Zhao Y, Zhang X, Li C, Zhang S. Practices for modeling oil shale pyrolysis and kinetics. Rev Chem Eng 2017;34:21–42.
[42] Romero-Sarmiento MF, Ramiro-Martinez S, Berthe G, Fleury M, Littke R. Geochemical and petrophysical source rock characterization of the Vaca Muerta formation: implications for unconventional resource estimations. Int J Coal Geol 2017;184:27–41.
[43] Romero-Sarmiento MF, Euzen T, Rolais S, Juang C, Littke R. Artificial thermal maturation of source rocks at different thermal maturity levels: applications to the Triassic and Doig formations in the western Canada sedimentary basin. Org Geochem 2016;97:148–62.
[44] Romero-Sarmiento MF, Pillot D, Letort G, Lamoureaux-Var V, Beaumont V, Huc AY, et al. New Rock-Eval method of unconventional shale reservoir systems. Rev Inst Français Pétrole Energy Nouv 2015;71:1–9.
[45] Romero-Sarmiento MF, Pillot D, Letort G, Lamoureaux-Var V, Beaumont V, Huc AY, Garcia B. New Rock-Eval method for characterization of shale plays. In: 14th Latin America Congress on Organic Geochemistry (ALAGO). Buzios, Rio de Janeiro-Brazil; 2014.
[46] Rezaee R, Saeedi A, Clennell B. Tight gas sands permeability estimation from mercury injection capillary pressure and nuclear magnetic resonance data. J Petrol Sci Eng 2012;88:92–9.
[47] Rueslåtten Håkon, Eidsemo T, Carsten Slot-Petersen. NMR studies of an iron-rich sandstone oil reservoir. In Proceeding of the 1998 International Symposium of Society of Core Analysts, papers, vol. 9821; 1998.
[48] Saif Tarik, Lin Qingyang, Bijeljic Branko, Blunt Martin J. Microstructural imaging and characterization of oil shale before and after pyrolysis. Fuel 2017;197:562–74.
[49] Saif Tarik, Lin Qingyang, Butcher Alan R, Bijeljic Branko, Blunt Martin J. Multi-scale multi-dimensional microstructure imaging of oil shale pyrolysis using X-ray micro-tomography, automated ultra-high-resolution SEM, MAPS Mineralogy and FIB-SEM. Appl Energy 2017;202:628–47.
[50] Sanei Hamed, Wood James M, Ardakani Omid H, Clarkson Christopher R, Jiang Chunqing. Characterization of organic matter fractions in an unconventional tight gas siltstone reservoir. Int J Coal Geol 2015;150:296–305.
[51] Smith MG, Bustin RM. Late Devonian and Early Mississippian Bakken and Exshaw black shale source rocks, Western Canada Sedimentary Basin: a sequence stratigraphic interpretation. AAPG Bull 2000;84:940–60.
[52] Solum MS, Mayne CL, Orendt AM, Pugmire RJ, Adams J, Fletcher TH. Characterization of macromolecular structure elements from a Green River oil shale, I. Extracts. Energy Fuels 2013;28:453–65.
[53] Sondergeld CH, Newsham KE, Comisky JT, Rice MC, Rai CS. Petrophysical considerations in evaluating and producing shale gas resources. SPE Unconventional Gas Conference. Society of Petroleum Engineers; 2010.
[54] Song Y-Q, Venkataramanan L, Hürlimann MD, Flaum M, Frulla P, Straley C. T1–T2 correlation spectra obtained using a fast two-dimensional Laplace inversion. J. Magn. Reson. 2002;154:261–8.
[55] Sonnenberg SA, Pramudito A. Petroleum geology of the giant Elm Coulee field, Williston Basin. AAPG Bull 2009;93:1127–53.
[56] Sulucarnain ID, Sondergeld CH, Rai CS. An NMR study of shale wettability and effective surface relaxivity. SPE Canadian Unconventional Resources Conference. Society of Petroleum Engineers; 2012.
[57] Tinni A, Sondergeld C, Rai C. NMR T 1-T 2 response of moveable and nonmoveable fluids in conventional and unconventional rocks. Avignon, France: International Symposium of Core Analysts; 2014. p. 8–11.
[58] Vandenbroucke M, Largeau C. Kerogen origin, evolution and structure. Org Geochem 2007;38:719–833.
[59] Washburn KE, Birdwell JE. Updated methodology for nuclear magnetic resonance characterization of shales. J Magn Reson 2013;233:17–28.
[60] Werner-Zwanziger U, Lis G, Mastalerz M, Schimmelmann A. Thermal maturity of type II kerogen from the New Albany Shale assessed by 13 C CP/MAS NMR. Solid State Nucl Magn Reson 2005;27:140–8.
[61] Witte E, Schenk H, Müller P, Schwochau K. Structural modifications of kerogen during natural evolution as derived from 13C CP/MAS NMR, IR spectroscopy and Rock-Eval pyrolysis of Toarcian shales. Org Geochem 1988;13:1039–44.
[62] Xu P. Truncated SVD methods for discrete ill-posed problems. Geophys J Int 1998;135:505–14.